Self-Aggregative Recognition and Extraction of Perfluorooctanesulfonate with Flexible Cationic Water-Soluble Deep Cavitands

Ria Lian,[1] Yu-Dong Yang,[4] Jose L. Moreno, Jr.,[1] Becky L. Eggimann,[2] Junyi Chen,[1] Lucas J. Gibson-Elias,[1] Christoper G. Williams,[1] Peixi Jiang,[1] Andrew J. Lee,[3] Leonard J. Mueller,[1] Jonathan. L. Sessler,[4]* J. Ilja Siepmann,[2]* Darren W. Johnson[3]* and Richard J. Hooley[1]*

[1]Department of Chemistry, University of California–Riverside, Riverside, CA 92521, U.S.A. [2] Department of Chemistry and Chemical Theory Center, University of Minnesota–Twin Cities, MN, 55455, U.S.A. [3] Department of Chemistry & Biochemistry, Materials Science Institute, Knight Campus for Accelerating Scientific Impact, University of Oregon, Eugene, OR 97403, U.S.A. [4] Department of Chemistry, The University of Texas at Austin, 105 East 24th Street, Stop A5300, Austin, TX 78712, U.S.A.

ABSTRACT: Cationic water-soluble deep cavitands enable hierarchical assembly-based recognition, optical detection and extraction of perfluoroalkyl substances (PFAS) in aqueous solution. Recognition of the PFAS occurs at the lower rim crown of the cavitand, which triggers self-aggregation of a PFAS-cavitand complex, allowing extraction from water. In addition, when paired with an indicator dye that can be bound in the cavity of the host molecule, the PFAS-cavitand association causes a significant (>20-fold at micromolar [PFAS]) enhancement of dye fluorescence due to conformational rearrangement of the fluxional cavitand **AMI**, allowing optical sensing of PFAS. The cavitands are water-soluble, and the detection and recognition occur in purely aqueous solution. The association is most effective for long chain sulfonate PFAS, and as such, selective optical detection of perfluorooctanesulfonate is possible, with a LOD = 130 nM in buffered water, and 500 nM in real-world samples such as polluted canal water. By pairing the **AMI** host with multiple dyes in an array-based format, full discrimination of five other PFAS can be achieved at micromolar concentration *via* differential sensing. In addition, the aggregation process allows extraction of PFAS from solution, and a 99% reduction of PFOS concentration in water is possible with a single treatment of an equimolar concentration of **AMI** cavitand. The hierarchical nature of the cavitand recognition system allows both selective, sensitive optical detection and extraction of PFAS from water with a single scaffold.

Introduction

Perfluoroalkyl substances (PFAS) represent a class of problematic environmental pollutants,[1] and there is a growing need for new methods to detect, recognize and extract them from drinking and wastewater,[2] as they have been implicated in a plethora of adverse health effects upon human consumption.[3] Detection strategies include instrumental methods such as LCMS, SERS or SPR.[4] Unfortunately, these methods, while effective, require complex and expensive instrumentation and laborious sample preparation. Optical detection, either colorometric or fluorescence-based,[5] is desirable for its simplicity; however, selectivity and sensitivity remain a challenge. Solid state sensors[6] (such as MOFs, nanoparticles or polymers, among others) can be effective, as can small molecule cations.[7] Nevertheless, at present the most adaptable solution-phase method of optical PFAS detection is indicator displacement-based[8] molecular recognition.[9] Macrocycles such as cyclodextrins,[2e] calixarenes[9a] or cyclophanes[9b] can be used to bind PFAS, and in the presence of a suitable dye molecule, indicator displacement can allow optical detection. The challenge with this approach is that individually tailored hosts need to be created for each specific size and shape of PFAS, and discriminating similarly structured variants is non-trivial. A particular challenge involves the development of a macrocycle-based sensor system capable of recognizing perfluorinated alkyl sulfonates (e.g., perfluorooctanosulfonate, PFOS). These species constitute a class of PFAS that have generally proven more challenging to sense than their carboxylic acid PFAS congeners.[2]

In addition to applications in optical detection, macrocycles have been used to extract PFAS from solution.[10] A notable example of this strategy was recently reported, whereby a cationic pillararene formed 1:10 complexes with added perfluoroalkanoate (PFA) salts, taking advantage of interactions between multiple adjacent PFA molecules in the assembly to drive affinity and selectivity.

Particularly appealing are systems that are capable of performing *both* optical detection *and* extraction using the same scaffold.[9a,11] If the host has two interdependent recognition motifs, i.e., a cavity for indicator binding and a separate motif that provides affinity for PFAS, combined sensing and capture applications are possible. We have shown that cationic water-soluble deep cavitands[12] can recognize a variety of anions at the lower rim crown of the host, from small anions, such as iodide,[12b] to non-canonically folded DNA strands.[12c-d] This lower rim recognition allosterically

regulates the conformation of the flexible cavity, modulating dye recognition and allowing selective anion detection in aqueous solution, and even serum. Here, we expand the scope of this recognition to the sensitive detection of PFAS in purely aqueous solution (including real-world water samples), with strong selectivity for long chain PFA sulfonic acids such as PFOS. The recognition process triggers self-aggregation of the cavitand:PFA complex to form insoluble aggregates that can be exploited for PFA sulfonate extraction from aqueous solution.

Results and Discussion

An advantage of using water-soluble deep cavitands for PFAS recognition is that they display two orthogonal recognition motifs (Figure 1) – the internal cavity and the pendant functionality, either at the upper rim or lower crown. Theoretically, PFAS could bind with the fluorous tail in the host cavity (as is the case for hydrocarbon lipids such as SDS, Figure 1), or in the anionic form at the lower rim *via* charge-charge interactions. Fluorocarbons can bind in related resorcinarene-based capsules,[13] and PFAS are bound in the cavity of calixarenes or other toroidal macrocycles.[9] Unfortunately, flexible cavitands, such as those shown in Figure 1, bind fluorous guests more weakly than the corresponding hydrocarbon species (for example, minimal affinity of PFOS is seen for the neutral precursor of **AMI** in $CDCl_3$; see Figures S-22 – S-23). As such, they are not ideally suited for high-performance PFAS recognition. However, a vital feature of the recognition behavior of deep cavitands is that they are highly aggregative in aqueous solution, and this can affect the fluorescence emission of indicator dyes bound in the cavity.[14] This propensity for aggregation allows multiple orthogonal recognition mechanisms to be exploited for enhanced target selectivity.

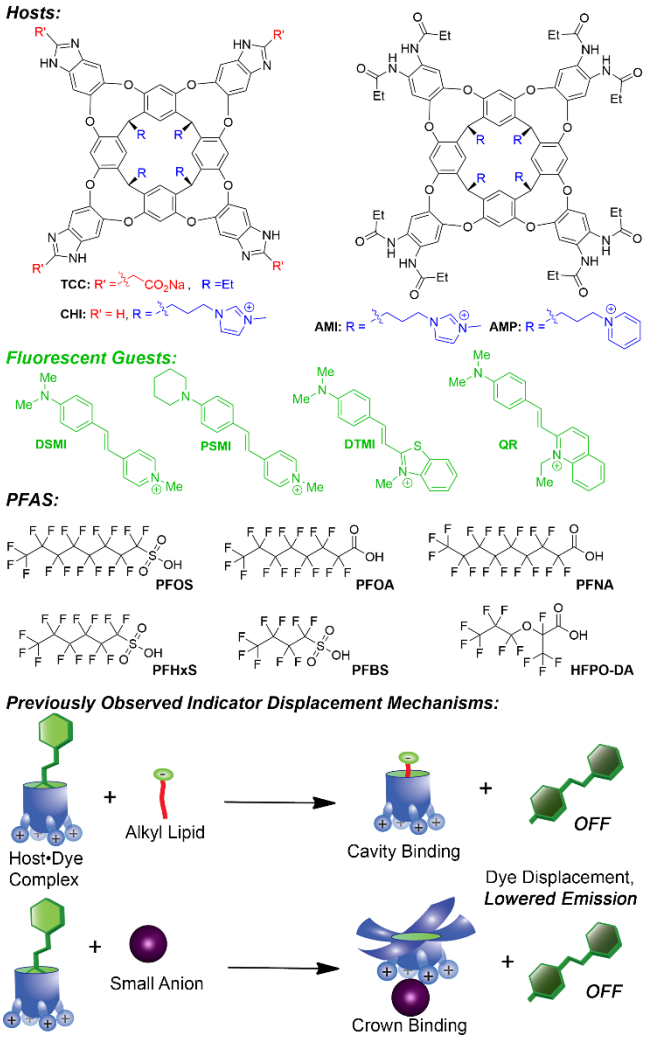

Figure 1. The structures of cavitand hosts, indicator dyes and PFA targets used in this study. Also shown are known cavitand-based recognition mechanisms. [12b, 15a]

In light of the above considerations, we tested a range of water-soluble deep cavitands and indicator dyes for their response to added PFAS (Figure 1). The cavitands tested were the anionic **TCC** (which is the most effective host for cavity-based binding of hydrophobic species[15]), and cationic hosts **AMI**, **CHI** and **AMP**,[16] which can bind anions such as iodide or DNA at the lower crown.[12b,c] These hosts vary in the nature of the lower rim cationic group (pyridinium or N-methyl imidazolium), as well as the cavity conformation: the octamide cavitands **AMI** and **AMP** are unfolded and maintain the "kite" conformation[17] in water in the absence of guest, whereas **CHI** remains folded and kinetically stable. The cavitands were paired with a series of styrylpyridinium dyes that have been shown to bind strongly in all tested hosts,[12] **DSMI, PSMI, DTMI** and Quinaldine Red (**QR**). A range of PFAS species that are anionic at neutral pH were selected as targets (see Figure 1). These included long chain sulfonates and carboxylates (PFOS, PFOA, PFNA), as well as shorter chain sulfonates (PFHxS, PFBS) and branched PFAS (HFPO-DA, also known as Gen-X).

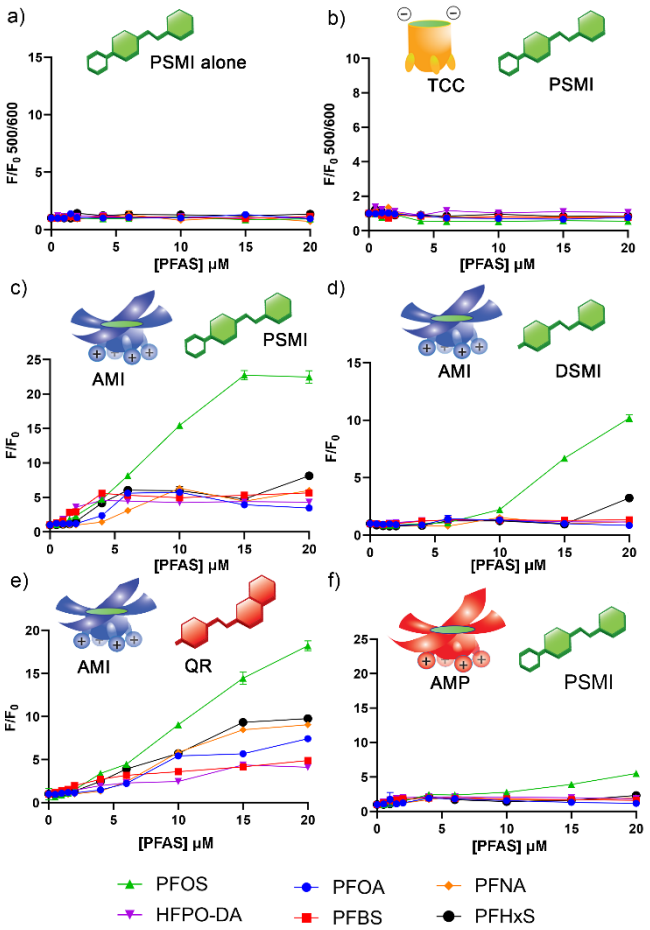

Figure 2. Fluorescence titration plots of different PFAS (0-20 μM) added to solutions of a) **PSMI** dye only, b) **TCC•PSMI**, c) **AMI•PSMI**, d) **AMI•DSMI**, e) **AMI•QR**, f) **AMP•PSMI** in 20 mM Tris buffer, pH = 7.4. [**cavitand**] = 4 μM, [**dye**] = 0.5 μM, F_0 = emission in the absence of PFAS.

The PFAS (0 – 20 μM) were titrated into a solution of detecting elements (i.e. individual cavitand:dye pairings, or the dyes alone) in 20 mM Tris buffer at pH 7.4. The results are shown in Figure 2, S-1 – S-4. As might be expected, no change in emission was seen when the PFAS were added to solutions of dye alone ([dye] = 0.5 μM; Figure 2a and Figure S-1). In addition, pairing the anionic **TCC** with dyes was also ineffective (Figure 2b), a finding rationalized in terms of the linear PFAS being unable to properly fill the cavity of **TCC** and thus being incapable of displacing the dyes from the host. The cationic **CHI** also proved ineffective in detecting the test PFAS considered in this study, showing only a relatively small and variable response (see Figure S-4).

Gratifyingly, the flexible cationic cavitand **AMI** showed a strong response to added PFAS (Figure 2c-e). However, the nature of the response was surprising, as titration of as little as 20 μM PFOS caused a substantial *increase* in emission of the **AMI•**dye pairing. Styrylpyridinium dyes have enhanced fluorescence when bound in these deep cavitands, so any indicator displacement should cause a decrease in fluorescence.[12] Similarly, we have shown that binding small anions at the lower rim crown causes a conformational switch in the cavitand that expels the dye, lowering the fluorescence emission intensity (see Figure 1 for a cartoon illustration).[12b] The response profile of increased emission intensity being observed upon adding PFOS was qualitatively similar with all the **AMI•**dye pairings tested, with the F/F_0 response varying from 10 (**DTMI**) to 23 (**PSMI**) when exposed to 20 μM PFOS (see Figures 2c-e and S-2, S-3). These increases in emission lead us to suggest that the recognition is not due to simple indicator displacement, either from cavity-based binding of the PFA tail or 1:1 binding of the PFA at the crown.

To interrogate the determinants leading to the increase in fluorescence intensity upon treatment with PFOS, we exposed the other PFAS targets to the same set of **AMI•**dye combinations (see Figures 2 and S-1 – S-4). The responses revealed that the **AMI•**dye recognition system is selective for PFOS, as it gives by far the largest increase in emission with each dye. On the other hand, the *selectivity* is dependent on the nature of the dye. For example, the **AMI•DSMI** complex is highly selective for PFOS – when 15 μM PFOS is added, F/F_0 = 6.7 (as opposed to F/F_0 (PFOA) = 1.0). In contrast, **AMI•QR** is far more responsive to all PFAS (Figure 2e), with F/F_0 (PFOS) = 14.4 and F/F_0 (PFOA) = 5.7 at [PFAS] = 15 μM. Other trends were observed, notably that sulfonate PFAS gave rise to higher responses than their carboxylic acid congeners. Moreover, the longer the perfluoroalkyl chain, the greater the fluorescence response when comparing PFAS with identical headgroups (i.e., PFA carboxylates vs. PFA sulfonates). In addition, the detection selectivity for PFOS was consistent in the presence of other PFAS – for example, adding PFOS to an **AMI•**PFOA**•PSMI** mixture caused an increase in emission, but the inverse, adding PFOA to **AMI•**PFOS**•PSMI** caused no change (see Figure S-16).

Changing the nature of the cationic group at the base of the cavitand was also found to affect the response – when **AMP** is used as host with **PSMI** as the dye, a positive response in emission is seen upon titration with the PFAS suite, with again PFOS causing the largest increase (Figure 2f). However, the magnitude of the response is far less than that seen with **AMI**. The variable responses of **CHI**, **AMI** and **AMP** show that PFAS detection is sensitive to the nature of both the lower rim crown group and the conformational flexibility of the water-soluble deep cavity.

As the PFAS detection involves the charged lower rim functional groups, we tested the effect of pH on the response. The various PFAS ([PFAS] = 1 – 20 μM) were added to 4 μM **AMI** in the presence of the dyes in buffered solutions at pH = 3.0, 5.5, 7.4 and 8.5 (see Figures S-2 – S-9). The fluorescence response for PFOS was lower at pH 3.0, but unchanged at pH 5.5. Moreover, all other PFAS gave almost identical responses under all four tested pH conditions. This result is not entirely unexpected, as PFAS are strong acids, and are essentially fully anionic over the 3.0-9.5 pH range. Thus, any charge interactions between the host crown (which has a static positive charge) and the PFAS will be retained in each case.

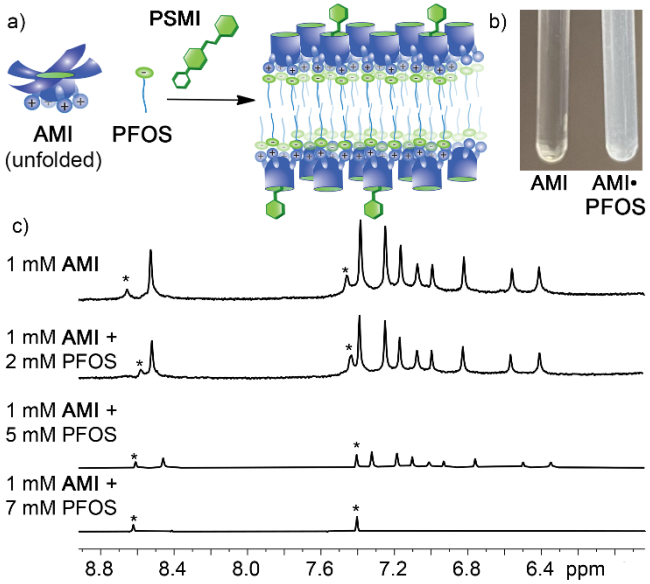

Figure 3. Cavitand-PFAS Aggregation. a) Schematic illustration of the proposed aggregation process and localization of the dye in the aggregate; b) image showing the precipitation that occurs when a 1 mM solution of cavitand **AMI** in D_2O is treated with 7 mM PFOS; c) ^{1}H NMR spectra of **AMI** recorded after the addition of varying concentrations of PFOS (400 MHz, D_2O, 298 K, * = residual N-methylimidazolium impurity from cavitand synthesis).

To better understand the recognition mechanism, the cavitand:PFAS binding was studied by NMR spectroscopy. Cavitand **AMI** was combined with PFOS in D_2O in two ways – either PFOS was sequentially added to a 1 mM D_2O solution of the cavitand, or the cavitand was added to a 1 mM D_2O solution of PFOS. In each case, ^{1}H NMR (Figures 3 and S-17 – S-18) and ^{19}F NMR (Figure S-19) spectral analyses revealed the disappearance of NMR signals for *both* the cavitand and the PFOS. As can be seen in Figure 3, no changes in chemical shift are seen in the **AMI** peaks as PFOS is added; however, their intensity drops until no **AMI**-derived signals are seen. In addition, significant aggregation and precipitation is observed in the NMR tube (Figure 3b). This occurs in both cases, irrespective of which component is added to which. Evidently the cationic cavitands bind the anionic PFAS at the lower rim crown, which triggers self-aggregation and formation of insoluble adducts at the mM concentrations necessary for NMR spectral studies. These experiments were repeated with different PFAS (namely PFOA) and different cavitands (**CHI**), and in each case, aggregation and precipitation was observed (see Figures S-20 – S-21). The aggregation process is poorly selective – at millimolar concentrations, all PFAS can aggregate with any cationic cavitand, indicating that the PFAS recognition is independent of indicator dye. In addition, the **AMI**-PFOS aggregation test was repeated in the presence of 0.5 mM **DSMI** dye (see Figures S-27 – S-28). In that case, the aggregation occurred as before, and the solid aggregate was colored by the dye while the aqueous solution remained colorless. No peaks for free **DSMI** were seen in the ^{1}H NMR spectrum after aggregation, illustrating that all of the dye (at this concentration, stoichiometry and NMR detection limit) is incorporated in the **AMI**•PFOS aggregate.

Solid-State NMR (ssNMR) spectral studies provided further support for the proposed aggregation. An **AMI•PFOS** sample in D_2O was collected via centrifugation at 5000 rpm and packed into an MAS rotor for ^{19}F ssNMR. Under 10 kHz MAS, the spectrum exhibited the expected ^{19}F peaks for PFOS in the solid state. In contrast, no ^{19}F signals were observed in the absence of MAS, indicating that to the limits of detection all the PFOS in this sample were present in the aggregated state, consistent with the lack of peaks seen in the solution-phase ^{19}F NMR spectral studies (see Figures S-29 – S-30). The terminal -CF_3 group showed a slight variation in chemical shift compared to PFOS free in aqueous solution. This is consistent with the CF_3 group experiencing a different chemical environment in the solid aggregate, as the result of being packed with other fluorous tails and hidden from water. Interestingly, two signals for the terminal CF_3 were observed, indicating the presence of discrete chemical and magnetic environments within the aggregate. The other CF_2 peaks in the spectrum showed smaller shift perturbations. Spatial proximity between the fluorine environments was indicated by cross-peaks in a 2D dipolar-driven ^{19}F-^{19}F correlation experiment.

The aggregates were further characterized by dynamic light scattering (DLS). Solutions of **AMI** (0.1 μM) and PFOA (0.4 μM) were combined in water and filtered through a 0.45 μm filter. No obvious large-sized particles were observed, therefore the process was repeated without filtration. The DLS plots (see Figures S-37 – S-40) revealed that the average radius of the **AMI•PFOA** aggregates was 2.6 μm, which explained their removal by the 0.45 μm filter. At the tested concentrations, both PFOA and **AMI** were slightly aggregated on their own, but only small amounts of <100 nm aggregates were seen. The proposed aggregation was also corroborated by zeta potential measurements, which revealed **AMI•PFOS** aggregates with a zeta potential of 1.9 mV (Figure S-42). Analysis by optical microscopy and transmission electron microscopy (Figures S-44 – S-45) showed the formation of micron-sized aggregates. The aggregates are not ordered, and do not form defined shapes. Nevertheless, the average size of the aggregates is consistent with the DLS studies, namely species of ~2 μm in diameter. This is consistent with the ^{19}F ssNMR spectral data, which shows that the PFOS is present in the solid state in multiple different environments, indicating a disordered aggregate.

The above findings enable a postulated mechanism for the recognition and sensing process (Figure 3a). The cationic cavitands allow coordination of multiple anionic PFAS at the lower crown – the strongly hydrophobic and weakly lipophobic character of these PFAS allows for self-aggregation into a layered structure, with a fluorous-rich domain formed in the assembly (in a similar manner as recently seen with functionalized pillar-[5]-arenes[10]). These aggregates are insoluble since the charged solubilizing groups in both the cavitand and the PFAS are now compensating

each other and also hidden from water. They thus precipitate from solution at higher concentrations. This behavior is observed for all cationic cavitands (**AMI**, **AMP** and **CHI**), independent of the nature of the cavity, and longer PFAS (e.g., PFOS vs. PFHxS and PFNA vs. PFOA) are more effective in triggering this aggregation.

The above aggregation mechanism does not explain the vast difference in fluorescence response between **AMI** and **CHI**, however, nor does it provide any insights into the cavitand:dye stoichiometry. To estimate the ratio of cavitands to PFOS in the aggregate, the effect of [PFOS] on the dye binding affinity of **AMI** was tested. The dye:host affinities are already known: K_d (**AMI-DTMI**) = 11.9 μM, K_d (**AMI-PSMI**) = 6.7 μM in 20 mM Tris buffer (pH 7.4).[12b] To determine the effect of PFOS on the affinity, cavitand **AMI** was titrated into a solution of either **PSMI** or **DTMI** dye (0.5 μM) in 20 mM Tris (pH 7.4) buffer with varying [PFOS] (0, 5, 10, 20 μM; see Figures 4 and S-11). The shape of the resulting plots was unexpected: In the presence of PFOS, the dye emission rises sharply and then plateaus. The plateaus occur at [**AMI**] ≈ 0.25 × [PFOS], i.e., in the presence of 20 μM PFOS, the **AMI•dye** emission plateaus at [**AMI**] ≈ 5 μM, whereas with 10 μM PFOS, the plateau occurs at [**AMI**] ≈ 2.5 μM, etc. On this basis, we conclude that the ratio of cavitand:PFOS in the aggregate is 1:4, i.e., each imidazolium group coordinates roughly one PFOS molecule. The overall charge of the **AMI•PFOS** complex is thus near-neutral.

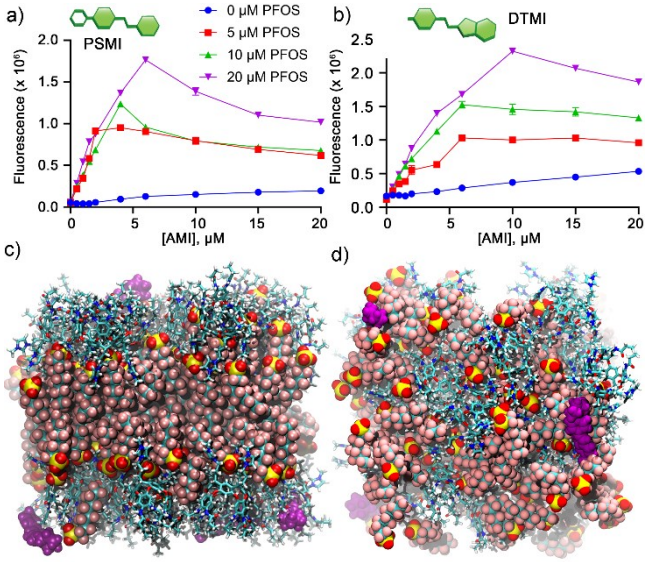

Figure 4. a,b) Fluorescence response of a) 0.5 μM **PSMI** dye; b) 0.5 μM **DTMI** dye seen upon addition of varying [**AMI**] in the presence of differing amounts of PFOS, 20 mM Tris buffer, pH = 7.4. c,d) Snapshot from molecular dynamics simulation of **AMI**-**PSMI**-PFOS assembly started from bilayer (c) and randomly mixed (d) configurations. Purple spheres highlight **PSMI** dyes, pink, yellow and red spheres show PFOS anions, and wireframe shows the **AMI** cavitands.

Unfortunately, the complexity of the self-assembly process precludes accurate determination of the **AMI-dye** affinity constant since the binding equations for a 1:1:4 complex cannot be solved in closed form. However, as a rudimentary estimate, the linear regions of the **AMI•dye** plots in the presence of 0/5/10/20 μM PFOS were subjected to a simple 1:1 binding affinity calculation using BindFit.[18] The fittings were obviously non-ideal, especially for the **DSMI** dye (see Figures S-11, S-12 and Table S-1 for the full dataset). Nevertheless, considered in concert, they reveal that there is no substantial increase in **AMI**-dye affinity in the presence of increasing [PFOS]. For example, in the presence of 20 μM PFOS, **PSMI** has an estimated K_d (**AMI**) = 5.5 μM, which is essentially the same as the K_d without PFOS (K_d = 6.7 μM[12b]). A similar trend was seen with **DTMI**. In this case, the affinity for **AMI** in the presence of 20 μM PFOS was estimated to be K_d = 10.4 μM. Again, this value is identical (within error) to that observed in the absence of PFOS (K_d = 11.9 μM[12b]).

The above observations could reflect the dye being bound simply in the hydrophobic PFOS aggregate. We consider this unlikely since no enhancement in dye emission was seen in the presence of any PFAS in the absence of cavitand (Figure 2a). Moreover, all these experiments were performed at concentrations far below the critical micelle concentration of PFOS. In addition, simply adding dye to hydrophobic micelles (either PFOS or a hydrocarbon lipid, SDS) at high concentration ([PFOS] = 1 mM) only produces a minor increase in the emission intensity (~1.5-fold). Specifically, the fluorescence of the dye alone is not enhanced by addition to micelles, it requires complexation in the cavitand host (see Figure S-14).

We rationalize the above findings in terms of the flexible nature of the **AMI** cavity. The estimated affinities of the styrylpyridinium dyes for **CHI** and **AMI** are relatively similar, on the order of K_d ~ 5-10 μM.[12b,d] There are obviously differences, and some outliers, but the dye affinities lie broadly within this small range. However, the emission enhancement seen when the dyes bind in **CHI** (and the related **TCC**) is vastly higher than in **AMI**.[12d] For example, **DTMI** shows a 15-fold enhancement upon binding in **CHI** in Tris buffer, whereas binding in **AMI** only causes a 3-fold increase (see Figure S-13). Emission enhancement in styrylpyridinium dyes can occur via a number of mechanisms, including solvatochromic effects (higher emission is seen in non-polar solvents), restricted rotation when bound, and π-stacking effects. While the exact mechanism for enhancement in cavitands is unclear, each of these factors is enhanced in a more "rigid" cavitand – the closer interaction between host walls and bound dye restricts dye rotation, prevents interactions between water molecules and the bound dye, and provides increased π-π interactions. **CHI** and **TCC** are held in the folded "vase" conformation by a seam of water molecules at the upper rim – the barrier to wall opening is on the order of 17 kcal mol^{-1}, depending on the guest.[19] In contrast, the intramolecular interactions of the amide seam in **AMI** are broken by water, and the barrier to wall opening is far lower.

When the **AMI**-PFOS aggregate is formed, the aggregated structure forces the **AMI** cavitands together (shown in cartoon form in Figure 3a), which adds packing effects into the system. It is not simple to observe cavitand wall motion in such a disordered aggregate, but it is reasonable to suggest that this packing favors the more closed form of

AMI. We have seen similar effects when incorporating **TCC** in lipid micelles and vesicles – the walls are squeezed together and guest exchange is slowed.[20] Thus, the **AMI**-PFOS aggregate mimics a "tighter" cavitand environment, and enables **AMI** to behave more like **CHI** – the host exists in a more closed state, providing the bound dye more protection from water. As a result, the emission enhancement of the dyes is increased when compared to that in free solution. While **CHI** is capable of forming aggregates with PFOS, it is already "rigid", so minimal further enhancement in dye-based emission is seen. In other words, this particular cavitand aggregates the PFAS molecules, but no change in emission is seen.

The other unusual aspect of this detection system is its selectivity for PFOS over other PFAS. We ascribe this to enhanced aggregation, driven by a combination of the greater acidity of the sulfonic acid groups (leading to stronger interactions with the N-methylimidazolium groups as the cavitand crown) paired with the overall insolubility of the target, which leads to favorable packing interactions in the aggregate. Presumably, this reflects the presence of enhanced fluorous-fluorous and solvophobic interactions. PFOS has a much lower solubility (680 mg/L at 25 ºC) than PFOA (9.5 g/L at 25 ºC)[21] and the other perfluoroalkanoates tested. It is also longer and less soluble than the other perfluoroalkylsulfonates tested, which further favors cavitand-triggered aggregation. However, the differences in emission shown by the different **AMI**-dye pairings are less easy to explain. While the added dye is present in the aggregate, it can reside in multiple positions: either in the **AMI** cavity, in the interstitial spaces between the hosts, or in the fluorous phase of the aggregate. All locations are possible, but the strong cavitand dependence on the dye fluorescence profiles leads us to suggest that the emission enhancement occurs mainly by dye binding in the cavitands in the **AMI**-PFOS aggregate. As the tested PFAS all cause aggregation with **AMI** to some extent, changes in the size and shape of the dye must lead to differences in the cavitand binding affinity and localization in the aggregate, leading to variable enhancement profiles with different PFAS.

The isolated state and aggregate structure were also analyzed using **AMI**-containing model systems by molecular dynamics simulations with the compounds represented by the Generalized Amber force field.[22] The setup of the simulations and the force field selection follows prior modeling studies of cavitand systems.[23] For full simulation details, see the Supporting Information. Figure 4 illustrates the aggregate sensing mechanism for a system composed of 32 **AMI** cavitands, 4 **PSMI** dye molecules, and 132 PFOS anions. When the system is initialized from a lamellar structure (Figure 4c), this morphology remains stable over a 1 μs trajectory. Some of the PFOS anions migrate into the **AMI**-rich region where they can compensate the charge of the dye. When the system is initialized with a random arrangement of the **AMI**, PFOS, and dye molecules (Figure 4d), then over the 1 μs trajectory a bi-continuous structure with AMI-rich and fluorous-rich regions forms. The dye molecules are present in the aggregate in several different motifs, that is, dyes are found in the cavity, the interstitial spaces between cavitands, and the fluorous region where the anionic sulfonate group is often in close proximity to the positively charged ring of the **PSMI** dye. The isolated cavitand in 0.02 M NaCl solutions remains in the vase conformation[17] with the amides rotating to open and close the cavity. We surmise that the change from aqueous environment to regions of low polarity in the lamellar or bi-continuous aggregate contributes to the enhanced fluorescence signal. We surmise that the change from aqueous environment to regions of low polarity in the lamellar or bi-continuous aggregate contributes to the enhanced fluorescence signal. To investigate the upper-rim rigidity of **AMI** in the three environments (isolated in water, lamellar aggregate, and bi-continuous aggregate), we have computed heat maps of the probability distribution of two characteristic N-N distances across the upper rim (Figure S-48). We observe that the upper rim of the isolated **AMI** undergoes only minor structural changes and prefers a square shape with both characteristic N-N distances close to 11 Å. In contrast, the **AMI** upper rim in the aggregates shows a much broader distribution ranging from distorted elliptical shapes (5 Å × 14 Å) to a more square shape. The regions of high probability density show a slight boomerang shape with the sum of the two characteristic N-N distances being larger for the less distorted square shape.

The performance of the cavitand-based recognition/detection was further tested. The limit of detection (LOD) for PFOS was calculated in multiple different environments (Figure 5a). In either Tris (pH = 7.4) or $Na_2B_4O_7$ (pH = 8.5) buffer, the LOD using the **AMI•PSMI** sensor was quite similar, with LOD = 130 nM and 150 nM, respectively. Adding other PFAS into the mixture caused only a slight reduction in detection efficacy: the LOD using the **AMI•PSMI** sensor for a 1:1:1 mixture of PFOS/PFOA/PFNA in Tris buffer (pH = 7.4) = 270 nm (see Figure S-15). The performance was also tested in a real-world sample of water taken from the Gage Canal in Riverside, CA. Each PFAS was spiked into the canal water solution, and added to the **AMI•PSMI** sensor, and the emission measured (see Figures 5a and S-10). As expected, due to the complexity of the medium, detecting PFOS in the canal water sample was slightly less effective than in buffer: LOD (PFOS, Canal water) = 530 nM. Also, the selectivity for PFOS over the other PFAS was lower in the canal water sample with **AMI•PSMI**. This finding is rationalized in terms of the detection of the other PFAS being enhanced in canal water (see Figure S-10), rather than extensive reduction in PFOS sensitivity.

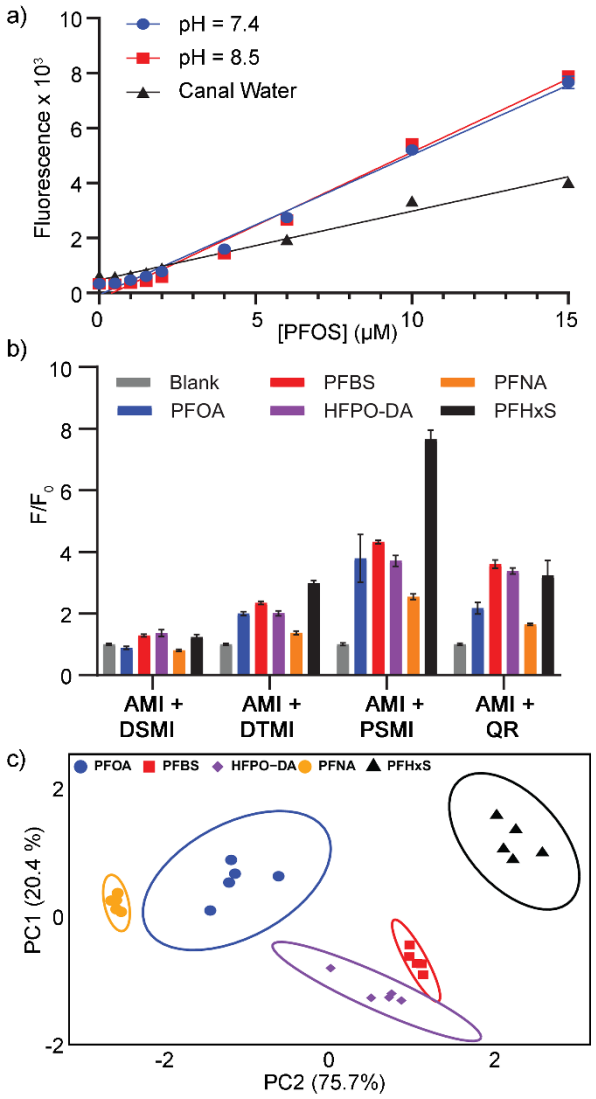

Figure 5. a) LOD determination for PFOS with **AMI•PSMI** in either 20 mM Tris (pH = 7.4) or 20 mM sodium borate (pH = 8.5) buffer or Gage canal water, Riverside, CA; b) fluorescence emission plots of 5 different PFAS (5 μM, not including PFOS) added to solutions of **AMI•dye** (20 mM Tris buffer, pH = 7.4) where **dye** = **DSMI, PSMI, DTMI or QR**; c) PCA scores plot generated from the data in part b), ellipses = 95% confidence limit. [**AMI**] = 4 μM, [**dye**] = 0.5 μM).

As noted above, the fluorescence response of the cavitand:dye system is dependent on the nature of the added dye. This dependence led us to explore the possibility for differential sensing. Accordingly, **AMI** was combined with the four different dyes in an array-based format. This technique is not necessary to differentiate PFOS from all the other PFAS since the selectivity for PFOS is strong; however, it allows for differentiation of the 5 non-PFOS targets. Fluorescence responses were recorded with four elements, consisting of the **AMI** cavitand and **DSMI**, **PSMI**, **DTMI** or **QR** in 20 mM Tris buffer (pH 7.4). The array elements were then exposed to either 2 μM PFAS or 5 μM PFAS. The responses were then subjected to Principal Component Analysis (PCA),[24] and the discrimination analyzed via scores plot (see Figures 5b,c and Figures S-32 – S-36 for the underlying sensing data). Full discrimination of the five PFAS targets for which no inherent selectivity is observed (i.e., PFOA, PFNA, PFBS, PFHxS and HFPO-DA) was achieved at [PFAS] = 5 μM using the full 4-element array. Specifically, the scores plot showed no overlap at the 95% confidence level for 5 repeats of each sample (Figure 5b). The discrimination was slightly less effective at [PFAS] = 2 μM, as some overlap in the PCA scores plot was seen for PFNA/PFOA and PFBS/HFPO-DA (Figure S-35). This overlap is understandable, considering the small difference in structure – PFNA and PFOA vary in only one CF_2 group. A more detailed analysis revealed that the **AMI•QR** element was essential to achieve discrimination. For instance, as underscored by the data shown in Figure 2c-e, when a 3-element array consisting of **AMI** and the **DSMI**/**PSMI**/**DTMI** dyes was used, complete discrimination was not seen at [PFAS] = 5 μM (Figure S-34). This reinforces the central concept of the sensing system, namely that the cavitand **AMI** triggers aggregation and that combining with the **DSMI**/**PSMI** dyes allows highly selective PFOS detection. In contrast, the use of the **QR** dye provides for a broader scope of PFAS detection.

The cavitand:PFAS aggregation also allows PFOS to be insolubilized in water, potentially permitting simple PFOS extraction and its removal from the aqueous phase. To test this possibility, samples of PFOS (10 μM, 5000 ppb) in phosphate-buffered saline (PBS, pH 7.4) were treated with an equimolar amount of **AMI** (10 μM) and the resulting aggregates filtered through a 0.22 μM methylcellulose ester (MCE) filter. The filtrate was subjected to high resolution LC-MS analysis (see Figure S-43) and compared to standard aqueous samples containing 1 or 10 ppb PFOS. These results showed that the PFOS concentration after a single, simple treatment was 43 ± 14 ppb (average of 3 experiments), corresponding to a 99% reduction of PFOS in the solution. This illustrates the two-fold nature of the recognition system: the aggregation process occurs at low concentrations in purely aqueous solution, allowing sensitive sensing when the **AMI** cavitand is paired with a dye. Conversely, insolubilization and extraction of the PFAS can be achieved by the cavitand in the absence of an added dye. Thus, one host system (**AMI**) can be used to both detect and extract PFAS from water by exploiting different facets of the same aggregation mechanism.

Conclusions

Here, we have shown that cationic water-soluble deep cavitands can selectively recognize perfluoroalkyl substances (PFAS) in aqueous solution. The recognition does not occur in the internal cavity of the host, but at the cationic lower rim. This triggers self-aggregation of PFAS-cavitand complexes in water, allowing simple extraction. As the cavity is unoccupied by the target, it allows the system to be paired with an indicator dye that can be bound in the cavity. Upon aggregation with PFAS, an allosteric change in **AMI** cavitand structure occurs, favoring dye binding and causing a large emission enhancement. This allosteric recognition enables selective and sensitive optical sensing of PFAS. The limit of detection for perfluorooctanesulfonate in buffered water is 130 nM, and 500 nM in

real-world samples such as polluted canal water. By pairing the **AMI** host with multiple dyes in an array-based format, full discrimination of five other PFAS can be achieved at micromolar concentrations *via* differential sensing. The aggregation process also allows extraction of PFAS from aqueous solution, specifically a 99% reduction in the [PFOS] is possible with a single treatment, using an equimolar concentration of **AMI** cavitand. The dual-mode nature of the cavitand recognition system allows both selective, sensitive optical detection and extraction of PFAS from water with a single scaffold.

ASSOCIATED CONTENT

Supporting Information

Experimental and statistical methods, fluorescence data, DLS and NMR spectral data. This material is available free of charge via the Internet at http://pubs.acs.org.

AUTHOR INFORMATION

Corresponding Authors

* E-mail: sessler@cm.utexas.edu, siepmann@umn.edu, dwj@uoregon.edu, richard.hooley@ucr.edu.

ACKNOWLEDGMENTS

This material is based upon work supported by the National Science Foundation under the Center for Aqueous Supramolecular Chemistry, CHE-2420332. J. L. S. thanks the Robert A. Welch Foundation for chair support (F-0018). B. L. E. and J. I. S. thank Jakob Schanzer for helpful discussions on molecular simulations of related cavitand systems.

REFERENCES

(1) (a) Fenton, S. E.; Ducatman, A.; Boobis, A.; DeWitt, J. C.; Lau, C.; Ng, C.; Smith, J. S.; Roberts, S. M. Per- and polyfluoroalkyl substance toxicity and human health review: current state of knowledge and strategies for informing future research. *Env. Tox. Chem.* **2020**, *40*, 606–630. (b) Wang, Y.; Darling, S. B.; Chen, J. Selectivity of per- and polyfluoroalkyl substance sensors and sorbents in water. *ACS Appl. Mater. Interfaces* **2021**, *13*, 60789–60814. (c) Wang, Z.; DeWitt, J. C.; Higgins, C. P.; Cousins, I.T. A never-ending story of per- and polyfluoroalkyl substances (PFASs)? *Environ. Sci. Technol* **2017,** *51*. 2508–2518.

(2) (a) Leung, S. C. E.; Wanninayake, D.; Chen, D.; Nguyen, N.-T.; Li, Q. Physicochemical properties and interactions of perfluoroalkyl substances (PFAS) - challenges and opportunities in sensing and remediation. *Sci. Total Environ.* **2023**, *905*, 166764. (b) Menger, R. F.; Funk, E.; Henry, C. S.; Borch, T. Sensors for detecting per- and polyfluoroalkyl substances (PFAS): a critical review of development challenges, current sensors, and commercialization obstacles. *Chem. Eng. J.* **2021**, *417*, 129133. (c) Kibbey, T. C. G.; O'Carroll, D. M.; Safulko, A.; Coyle, G. Multi-class machine learning classification of PFAS in Environmental water samples: a blinded test of performance on unknowns. *Environ. Sci. Adv.* **2024**, *3*, 366–382. (d) Shojaei, M.; Kumar, N.; Guelfo, J. L. An integrated approach for determination of total per- and polyfluoroalkyl substances (PFAS). *Environ. Sci. Technol.* **2022**, *56*, 14517–14527. (e) Chen, Z.; Lu, Y.-L.; Wang, L.; Xu, J.; Zhang, J.; Xu, X.; Cheng, P.; Yang, S.; Shi, W. Efficient recognition and removal of persistent organic pollutants by a bifunctional molecular material. *J. Am. Chem. Soc.* **2023**, *145*, 260–267.

(3) (a) Sunderland, E.M.; Hu, X.C.; Dassuncao, C.; Tokranov, A. K.; Wagner, C. C.; Allen, J. G. A review of the pathways of human exposure to poly- and perfluoroalkyl substances (PFASs) and present understanding of health effects. *J. Expo. Sci. Environ. Epidemiol.* **2019**, *29*, 131–147. (b) Wee, S. Y.; Aris, A. Z. Revisiting the "Forever Chemicals", PFOA and PFOS Exposure in Drinking Water. *npj Clean Water* **2023**, *6*, 57. (c) Gomis, M. I.; Vestergren, R.; Borg, D.; Cousins, I. T. Comparing the toxic potency in vivo of long-chain perfluoroalkyl acids and fluorinated alternatives. *Environ. Int.* **2018**, *113*, 1–9. (d) Luo, Y.; Li, X.; Li, J.; Gong, X.; Wu, T.; Li, X.; Li, Z.; Zhai, Y.; Wei, Y.; Wang, Y.; Jiang, G. Prenatal exposure of PFAS in cohorts of pregnant women: identifying the critical windows of vulnerability and health implications. *Environ. Sci. Technol.* **2024**, *58*, 13624–13635. (e) Fischer, F. C.; Ludtke, S.; Thackray, C.; Pickard, H. M.; Haque, F.; Dassuncao, C.; Endo, S.; Schaider, L.; Sunderland, E. M. Binding of per- and polyfluoroalkyl substances (PFAS) to serum proteins: implications for toxicokinetics in humans. *Environ. Sci. Technol.* **2024**, *58*, 1055–1063.

(4) Al Amin, M.; Sobhani, Z.; Liu, Y.; Dharmaraja, R.; Chadalavada, S.; Naidu, R.; Chalker, J. M.; Fang, C. Recent advances in the analysis of per- and polyfluoroalkyl substances (PFAS) – a review. *Env. Tech. Innovation* **2020**, *19*, 100879.

(5) Concellón, A.; Swager, T. M. Detection of Per- and polyfluoroalkyl substances (PFAS) by interrupted energy transfer. *Angew. Chem. Int. Ed.* **2023**, *62*, e202309928.

(6) (a) Niu, H.; Wang, S.; Zhou, Z.; Ma, Y.; Ma, X.; Cai, Y. Sensitive colorimetric visualization of perfluorinated compounds using poly(ethylene glycol) and perfluorinated thiols modified gold nanoparticles. *Anal. Chem.* **2014**, *86*, 4170–4177. (b) Dalapati, R.; Hunter, M.; SK, M.; Yang, X.; Zang, L. fluorescence turn-on detection of perfluorooctanoic acid (PFOA) by perylene diimide-based metal–organic framework. *ACS Appl. Mater. Interfaces* **2024**, *16*, 32344–32356. (c) Concellón, A.; Castro-Esteban, J.; Swager, T. M. Ultratrace PFAS detection using amplifying fluorescent polymers. *J. Am. Chem. Soc.* **2023**, *145*, 11420-11430. (d) Chen, B.; Yang, Z.; Qu, X.; Zheng, S.; Yin, D.; Fu, H. Screening and discrimination of perfluoroalkyl substances in aqueous solution using a luminescent metal–organic framework sensor array. *ACS Appl. Mater. Interfaces* **2021**, *13*, 47706–47716.

(7) Yang, Y.-D.; Zhang, Q. Jin, X.; Chau, C. V.; Yang, J.; Henkelman, G.; Chi, X.; Gong, H.-Y.; Hooley, R. J.; Sessler, J. L. Readily visualized perfluorooctanoic acid detection using a small molecule chemosensor. *Angew. Chem. Int. Ed.* **2025**, *64*, e202501245.

(8) (a) You, L.; Zha, D.; Anslyn, E.V. Recent advances in supramolecular analytical chemistry using optical sensing. *Chem. Rev.* **2015**, *115*, 7840–7892. (b) Sedgwick, A. C.; Brewster, J. T.; Wu, T.; Feng, X.; Bull, S. D.; Qian, X.; Sessler, J. L.; James, T. D.; Anslyn, E. V.; Sun, X. Indicator displacement assays (IDAs): the past, present and future. *Chem. Soc. Rev.* **2021**, *50*, 9–38.

(9) (a) Zheng, Z.; Yu, H.; Geng, W.-C.; Hu, X.-Y.; Wang, Y.-Y.; Li, Z.; Wang, Y.; Guo, D.-S., Guanidinocalix[5]arene for sensitive fluorescence detection and magnetic removal of perfluorinated pollutants. *Nat. Commun.* **2019**, *10*, 5762. (b) Harrison, E. E.; Waters, M. L. Detection and differentiation of per- and polyfluoroalkyl substances (PFAS) in water using a fluorescent imprint-and-report sensor array. *Chem. Sci.* **2023**, *14*, 928–936.

(10) Gao, T.-N.; Huang, S.; Nooijen, R.; Zhu, Y.; Kociok-Köhn, G.; Stuerzer, T.; Li, G.; Bitter, J. H.; Salentijn, G. I. J.; Chen, B.; Miloserdov, F. M.; Zuilhof, H. Rim-based binding of perfluorinated acids to pillararenes purifies water. *Angew. Chem. Int. Ed.* **2024**, e202403474.

(11) He, Y.; Luo, D.; Lynch, V. M.; Ahmed, M.; Sessler, J. L.; Chi, X. Porous adaptive luminescent metallacage for the detection and removal of perfluoroalkyl carboxylic acids. *Chem* **2023**, *9*, 93–101.

(12) (a) Zhong, W.; Hooley, R. J. Combining excellent selectivity with broad target scope: biosensing with arrayed deep cavitand hosts. *Acc. Chem. Res.* **2022**, *55*, 1035–1046. (b) Hickey, B. L.; Raz, A. A. P.; Chen, J.; Moreno, Jr., J. L.; Hartman, J. D.; Zhong, W.; Hooley, R. J. Selective anion recognition and sensing in high salt water with cationic deep cavitands. *Chem. Commun.* **2023**, *59*, 7819–7822. (c) Chen, J.; Gill, A.D.; Hickey, B. L.; Gao, Z.; Cui, X.; Hooley, R. J.; Zhong, W. Machine learning aids classification and

discrimination of non-canonical DNA folding motifs by an arrayed host:guest sensing system. *J. Am. Chem. Soc.* **2021**, *143*, 12791–12799. (d) Chen, J.; Hickey, B.L.; Raz, A. A. P.; Gao, Z.; Hooley, R. J.; Zhong, W. Sensing base modifications in non-canonically folded DNA with an optimized host:guest sensing array. *ACS Sens.* **2022**, *7*, 2164–2169. (e) Chen, J.; Hickey, B. L.; Wang, L.; Lee, J.; Gill, A.D.; Favero, A.; Pinalli, R.; Dalcanale, E.; Hooley, R. J.; Zhong, W. Selective discrimination and classification of G-quadruplex structures with a host:guest sensing array. *Nat. Chem.* **2021**, *13*, 488–495.

(13) Purse, B. W.; Rebek, J., Jr. Encapsulation of oligoethylene glycols and perfluoro-n-alkanes in a cylindrical host molecule. *Chem. Commun.* **2005**, *41*, 722–724

(14) Liu, Y.; Perez, L.; Mettry, M.; Easley, C. J.; Hooley, R. J.; Zhong, W. Self-aggregating deep cavitand acts as a fluorescence displacement sensor for lysine methylation. *J. Am. Chem. Soc.* **2016**, *138*, 10746–10749. (b) Liu, Y.; Lee, J.; Perez, L.; Gill, A. D.; Hooley, R. J.; Zhong, W. Selective sensing of phosphorylated peptides and monitoring kinase and phosphatase activity with a supramolecular tandem assay. *J. Am. Chem. Soc.* **2018**, *140*, 13869–13877.

(15) (a) Trembleau, L.; Rebek, J., Jr. Helical conformation of alkanes in a hydrophobic cavitand. *Science* **2003**, *301*, 1219–1220. (b) Hooley, R.J.; Van Anda, H. J.; Rebek, J., Jr. Extraction of hydrophobic species into a water-soluble synthetic receptor. *J. Am. Chem. Soc.*, **2007**, *129*, 13464–13473.

(16) Mosca, S.; Yu, Y.; Rebek, J., Jr. Preparative scale and convenient synthesis of a water-soluble, deep cavitand. *Nat. Protoc.* **2016**, *11*, 1371–1387.

(17) Moran, J. R.; Ericson, J. L.; Dalcanale, E.; Bryant, J. A.; Knobler, C. B.; Cram, D. J. Vases and kites as cavitands. *J. Am. Chem. Soc.* **1991**, 113, 5707–5714.

(18) (a) www.supramolecular.org. (b) Hibbert, D. B.; Thordarson, P. The death of the Job plot, transparency, open science and online tools, uncertainty estimation methods and other developments in supramolecular chemistry data analysis. *Chem. Commun.* **2016**, *52*, 12792–12805. (c) Thordarson, P. Determining association constants from titration experiments in supramolecular chemistry. *Chem. Soc. Rev.* **2011**, *40*, 1305–1323.

(19) Hooley, R.J.; Van Anda, H. J.; Rebek, J., Jr. Extraction of hydrophobic species into a water-soluble synthetic receptor. *J. Am. Chem. Soc.*, **2007**, *129*, 13464–13473.

(20) Perez, L.; Mettry, M.; Caulkins, B.G.; Mueller, L.J.; Hooley, R.J. Lipid bilayer environments control exchange kinetics of deep cavitand hosts and enhance disfavored guest conformations. *Chem. Sci.* **2018**, *9*, 1836 – 1845.

(21) Alexander, J.; Auðunsson, G. A.; Benford, D.; Cockburn, A.; Cravedi, J.-P.; Dogliotti, E.; Di Domenico, A.; Fernández-Cruz, M. L.; Fink-Gremmels, J.; Fürst, P.; Galli, C.; Grandjean, P.; Gzyl, J.; Heinemeyer, G.; Johansson, N.; Mutti, A.; Schlatter, J.; van Leeuwen, R.; van Peteghem, C.; Verger, P. Perfluorooctane sulfonate (PFOS), perfluorooctanoic acid (PFOA) and their salts. Scientific Opinion of the Panel on Contaminants in the Food Chain. *The EFSA Journal* **2008**, *653*, 7-131.

(22) Wang, J.; Wolf, R. M.; Caldwell, J. W.; Kollman, P. A.; Case, D. A. Development and testing of a general AMBER force field. *J. Comp. Chem.*, **2004**, *25*, 1157-1174.

(23) Barnett, J. W.; Tang, D.; Gibb, B. C.; Ashbaugh, H. S. Alkane guest packing drives switching between multimeric deep-cavity cavitand assembly states. *Chem. Commun.*, **2018**, *54*, 2639–2642.

(24) Stewart, S.; Ivy, M. A.; Anslyn, E. V. The Use of Principal Component Analysis and Discriminant Analysis in Differential Sensing Routines. *Chem. Soc. Rev.* **2014**, *43*, 70–84.

TOC Graphic:

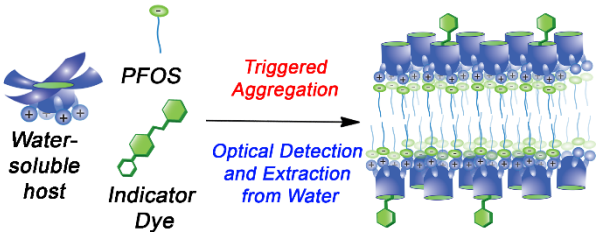
PFOS
Triggered
Aggregation
Water-
soluble
host
Indicator
Dye
Optical Detection
and Extraction
from Water